MENTORSHIP, SCHOLARSHIP, AND SERVICE: A SPECIAL ISSUE HONOURING PROFESSOR ADAMU N. BABA-KUTIGI, FNIP ON HIS RETIREMENT
FUDMA Journal of Sciences (FJS)
ISSN online: 2616-1370
ISSN print: 2645 - 2944
Vol. 10 ANB-K Special Issue, 2026, pp 106 – 117
DOI: https://doi.org/10.33003/fjs-2026-10(ANB-K)-5324

Radiological Assessment and Inhabitants Risk Evaluation of Primordial Radionuclides in Soils of Tambuwal LGA, Nigeria

***[1]Yusuf M. Ahijjo, [2]Adamu N. Baba-Kutigi, [3]Mazhar Hussain, [2]Adamu Idris, [4]Dahiru Dahuwa and [5]Umar Aminu**

[1]Department of Physics, Usmanu Danfodiyo University, P.M.B. 2346, Sokoto, Sokoto State, Nigeria.
[2]Department of Physics, Federal University, Dutsin-Ma, Katsina State, Nigeria.
[3]Department of Physics, GC University, Lahore, Pakistan.
[4]Department of Physics, Federal University of Health Sciences, Azare, Bauchi State. Nigeria.
[5]Department of Physics, Federal University of Medicine and Medical Sciences, Abeokuta, Ogun State, Nigeria.

*Corresponding authors' email: yusuf.musa@udusok.edu.ng

ABSTRACT
Natural background radiation from primordial radionuclides in soil represents a significant component of public radiation exposure, particularly in regions with distinctive geochemical compositions. This study systematically evaluated the baseline activity inventory of primordial radionuclides in surficial soil across Tambuwal, Sokoto State, Nigeria, and quantified associated terrestrial gamma radiation exposure to the local population. Activity concentrations of ^{226}Ra, ^{232}Th, and ^{40}K were measured using high-resolution gamma-ray spectrometry with a Hyperpure Germanium (HPGe) detector. Activity ranges were 19.50–125.50 $Bq{\cdot}kg^{-1}$ for ^{226}Ra, 21.90–62.50 $Bq{\cdot}kg^{-1}$ for ^{232}Th, and 278.04–815.03 $Bq{\cdot}kg^{-1}$ for ^{40}K. The mean ^{226}Ra concentration (73.68 $Bq{\cdot}kg^{-1}$) exceeded the UNSCEAR world average (35.0 $Bq{\cdot}kg^{-1}$) by more than twofold, while mean ^{40}K activity (648.66 $Bq{\cdot}kg^{-1}$) markedly surpassed the global average (420 $Bq{\cdot}kg^{-1}$); conversely, mean ^{232}Th activity (42.00 $Bq{\cdot}kg^{-1}$) was comparable to the world average (45 $Bq{\cdot}kg^{-1}$). This distinctive enrichment pattern reflects the local soil matrix geochemistry. The mean radium equivalent activity (Ra_{eq} = 183.68 $Bq{\cdot}kg^{-1}$) was below the recommended limit of 370 $Bq{\cdot}kg^{-1}$. Both mean external (H_{ex} = 0.50) and internal (H_{in} = 0.70) hazard indices satisfied the safety threshold of unity. The mean absorbed dose rate (86.45 $nGy{\cdot}h^{-1}$) and annual effective dose (106.03 $\mu Sv{\cdot}y^{-1}$) exceeded global benchmarks (~57 $nGy{\cdot}h^{-1}$ and 100 $\mu Sv{\cdot}y^{-1}$, respectively). Although, hazard indices remain within permissible limits, the moderately elevated dose metrics indicate signals warranting periodic monitoring. These findings establish Tambuwal as a moderate radiological risk zone, providing a critical georeferenced baseline for nuclear safety evaluations and evidence-based environmental management in northwestern Nigeria.

Keywords: Gamma-ray Spectrometry, Primordial Radionuclides, Hazard Indices, Tambuwal, Radiation Protection, Soil Sample

INTRODUCTION

The mining of globally sought-after industrial minerals, including kaolin and gypsum, has intensified globally including some regions of northwestern Nigeria due to the pressures of a burgeoning global economy (Adewumi *et al.*, 2026). Tambuwal Local Government Area (LGA) and its surroundings fall into one of the primary hubs for these activities, where artisanal and small-scale miners have operated for decades within mineralized rock formations. While these activities drive local economic growth, the disturbance of the Earth's crust facilitates the migration of naturally occurring radioactive materials (NORM) from the lithosphere to the biosphere (Banerjee *et al.*, 2025). This environmental shift raises significant concerns regarding occupational and public radiological exposure in mining communities and adjacent settlements.

The fundamental framework of this study is grounded in the internationally harmonized radiation protection principles established by the International Commission on Radiological Protection (ICRP), the International Atomic Energy Agency (IAEA), and the United Nations Scientific Committee on the Effects of Atomic Radiation (UNSCEAR). Central to this paradigm is the ALARA (As Low As Reasonably Achievable) principle, which seeks to prevent deterministic effects such as tissue damage from acute or prolonged exposure and minimize the probability of stochastic effects, primarily carcinogenesis and hereditary disorders (Adewumi *et al.*, 2026; Taiwo *et al.*, 2023). Natural radioactivity, which accounts for approximately 85% of the global effective dose of ionizing radiation, is primarily derived from four distinct categories: primordial, cosmogenic, internal (intra-body), and anthropogenic sources. In the context of terrestrial mining, the radiological burden is dominated by primordial radionuclides, specifically the ^{238}U (uranium) and ^{232}Th (thorium) decay series, alongside the non-series ^{40}K (potassium) (Ilori & Chetty, 2023). Exposure pathways in these environments are multifaceted, encompassing external gamma radiation from mineralized ores and waste rocks, inhalation of alpha-emitting radionuclides in respirable dust, and the ingestion of radon (^{222}Rn) and thoron (^{220}Rn) decay products (Adewumi *et al.*, 2026; Lucas, 2021).

Despite the documented prevalence of minerals like limestone, talc, and silicate minerals in construction and industrial sectors, systematic radiological data for the Tambuwal region remains sparse. Current literature often lacks site-specific baseline data for ^{238}U, ^{226}Ra, and ^{40}K, leaving a critical gap in our understanding of the long-term health implications for local populations (Adewumi *et al.*, 2026). This study addresses this lacuna by quantifying activity concentrations and estimating international hazard indices such as the radium equivalent activity (R_{aeq}) and annual effective dose (AED) to evaluate the risk profiles associated with unregulated artisanal mining. The findings are intended to inform regional radiation protection policies and

establish a robust baseline for environmental monitoring in West African resource exploitation areas.

MATERIALS AND METHODS

Soil Sampling Strategy and Collection Protocol

The rigorous characterization of environmental radioactivity in mining-impacted terrains demands a sampling protocol that is not only statistically robust but also harmonised with internationally validated methodologies for the measurement of naturally occurring radioactive materials (NORM) and technologically enhanced naturally occurring radioactive materials (TENORM) (IAEA, 2004 & ISO, 2023). The disturbance of geological formations during artisanal and small-scale mining operations facilitates the redistribution of primordial radionuclides from the lithosphere to surficial soil horizons, thereby altering the natural background radiation field and elevating both occupational and public exposure pathways (Tran, 2025 & IAEA, 2024). Consequently, the acquisition of representative soil samples with demonstrable spatial fidelity, sample homogeneity, and statistical validity constitutes the foundational prerequisite for any defensible radiological assessment (U.S. NRC, 2013 & ISO, 2017).

Soil sampling was conducted in strict accordance with the harmonised guidelines established by the IAEA for environmental radioactivity assessment and the ISO 18589 series for the measurement of radioactivity in soil (IAEA, 2004 & ISO, 2007), with particular emphasis on spatial representativeness, sample homogeneity, and statistical validity. A stratified random sampling design was employed to ensure proportional representation of the target population across five distinct mining sites within Tambuwal LGA, Sokoto State, Nigeria. This approach is consistent with the probabilistic sampling frameworks recommended for environmental monitoring programmes, wherein sampling locations are selected to capture the heterogeneity of anthropogenically disturbed terrains while maintaining geographical dispersion and statistical independence (ICRU, 2006 & ISO, 2017). Inter-site distances of approximately 25 km were maintained to preclude spatial autocorrelation and to ensure that each sampling unit constituted an independent observational entity (U.S. NRC, 2013).

At each designated sampling point, composite soil samples were extracted from surface deposits (0 cm depth) corresponding to excavated material stockpiles. The collection of composite samples from multiple discrete subsamples within a constrained spatial radius is a well-established practice in radiological surveys, as it effectively reduces the variance associated with small-scale spatial heterogeneity while providing a more reliable estimate of the mean contamination level (IAEA, 2005 & ISO, 2018). Accordingly, three discrete subsamples were collected within a 50 cm radius and thoroughly homogenised to achieve ≥95% spatial representativeness for each location. This subsampling density aligns with the envelope sampling approach advocated by the IAEA ALMERA network for the characterisation of NORM-impacted soils (IAEA, 2024a, 2024b). Sample mass was standardised to 2.5 kg (wet weight) to ensure sufficient material for subsequent gamma spectrometric analysis while maintaining geometric consistency for detector calibration and counting efficiency calculations (ISO, 2007, 2017).

All samples were immediately transferred to 300 ml polyethylene containers, assigned unique alphanumeric codes, and hermetically sealed to prevent cross-contamination, moisture loss, and radon ingress during transport to the analytical facility (IAEA, 2004, 2022). The hermetic sealing of soil samples is a critical quality assurance measure, as it preserves the secular equilibrium between ^{226}Ra and its short-lived progeny particularly ^{214}Pb and ^{214}Bi which is essential for the accurate quantification of radium activity by gamma-ray spectrometry (IAEA, 2023, 2024c). Furthermore, the implementation of a rigorous chain-of-custody protocol, encompassing detailed sample documentation and tamper-evident sealing, ensures the traceability and integrity of the analytical data from field collection through to laboratory measurement, thereby satisfying the quality control requirements stipulated under ISO/IEC 17025 for testing and calibration laboratories (ISO, 2017).

Sample Preparation and Pre-treatment

Upon arrival at the radiometric laboratory, all collected samples were subjected to a rigorous pre-treatment protocol designed to ensure analytical precision, radionuclide homogeneity, and reproducibility during high-resolution gamma spectrometric measurements. The samples were initially air-dried under controlled ambient laboratory conditions for approximately seven days in order to reduce inherent moisture content and minimize physicochemical alterations that could influence radionuclide distribution within the matrix. Thereafter, visible extraneous materials, including lithic fragments, plant residues, root fibers, and other organic detritus, were carefully removed manually to eliminate potential sources of analytical bias and matrix inhomogeneity (Wilson *et al.,* 2019 & Mauz *et al.,* 2022).

To further eliminate residual pore moisture while preserving the integrity of naturally occurring radionuclides, the samples were oven-dried at 75°C for 24 h using a thermostatically regulated convection oven. The selected drying temperature was intentionally maintained below volatilization thresholds for environmentally relevant radionuclides in order to avoid thermal losses and spectral distortions during subsequent gamma counting procedures (Lakosi *et al.,* 2018; Mauz *et al.,* 2022).

The dried materials were subsequently pulverized using an agate mortar and pestle to avoid metallic contamination and ensure effective particle size reduction. Homogenization was then achieved through thorough mechanical mixing prior to sieving with a 2.5 mm stainless-steel mesh using a vibratory sieve shaker. This treatment enhances sample uniformity, minimizes self-attenuation effects, and improves counting geometry consistency, which are critical parameters in low-background gamma spectrometry of environmental matrices (Tzortzis & Tsertos, 2003; Zsigrai *et al.,* 2015).

Exactly 250 mL of each processed sample was transferred into pre-cleaned Marinelli beakers of identical geometry to maintain detector efficiency consistency throughout the analytical campaign. The containers were hermetically sealed using polyvinyl chloride (PVC) tape and parafilm in order to prevent atmospheric exchange of gaseous radionuclides, particularly ^{222}Rn and ^{220}Rn, and to preserve radioactive progeny within the uranium and thorium decay chains. The sealed samples were subsequently stored for a minimum period of 28 days to allow restoration of secular radioactive equilibrium between parent radionuclides and their short-lived decay products prior to gamma spectrometric analysis (Lin & Harbottle, 1992; Wilson *et al.,* 2019 & Mauz *et al.,* 2022).

This standardized preparation methodology is widely recognized as essential for achieving reliable activity concentration measurements in environmental radioactivity investigations and for minimizing uncertainties associated with detector efficiency calibration, radionuclide migration,

moisture correction, and counting geometry effects (Nguyen & Zsigrai, 2005; Kurnaz *et al.,* 2007 & Gilmore, 2008).

Secular Equilibrium Considerations

To ensure radiometric accuracy and analytical reliability during gamma spectrometric quantification, all sealed samples were stored for a minimum duration of 28 days prior to counting in order to establish secular radioactive equilibrium between parent radionuclides and their short-lived progeny within the natural decay series. This equilibration interval is particularly critical for the ^{238}U decay chain, where the activity concentration of ^{226}Ra is commonly inferred indirectly through the gamma emissions of its daughter products, notably ^{214}Pb and ^{214}Bi. Following hermetic sealing, radioactive equilibrium is progressively attained through the in-growth of ^{222}Rn and its subsequent progeny, thereby enabling stable and reproducible photopeak intensities suitable for quantitative analysis (Gilmore, 2008 & Knoll, 2010).

The selected equilibration period exceeds seven half-lives of ^{222}Rn ($t_{1/2}$ = 3.82 d), thereby ensuring near-complete radioactive ingrowth and equilibrium stabilization between ^{226}Ra, ^{222}Rn, ^{214}Pb, and ^{214}Bi within the sealed counting geometry. This procedure is widely adopted in environmental radioactivity investigations because radon escape during sample preparation or storage can significantly compromise uranium-series activity determination and introduce substantial systematic uncertainties in detector calibration and radionuclide quantification (Debertin & Helmer, 1988; Wilson *et al.,* 2019 & Mauz *et al.,* 2022).

In contrast, the ^{232}Th decay series achieves equilibrium considerably more rapidly owing to the extremely short half-life of ^{220}Rn (thoron; $t_{1/2}$ = 55.6 s). Consequently, transient disequilibrium effects within the thorium series are negligible under properly sealed conditions, and prolonged storage contributes minimally to additional ingrowth stabilization. Under these circumstances, radionuclides such as ^{212}Pb, ^{228}Ac, and ^{208}Tl rapidly attain equilibrium with their respective progenitors, thereby facilitating reliable thorium activity assessment shortly after sample encapsulation (Tzortzis & Tsertos, 2003 & IAEA, 2020).

Unlike the uranium and thorium decay chains, ^{40}K exists as an independent primordial radionuclide that decays directly without generating long-lived radioactive daughters capable of influencing gamma spectrometric measurements. Accordingly, no equilibration correction or storage-related ingrowth considerations are required for potassium activity determination, and its characteristic 1460.8 keV gamma emission can be measured directly following sample preparation (Kurnaz *et al.,* 2007 & UNSCEAR, 2020).

The establishment of secular equilibrium prior to counting remains a fundamental requirement in low-background environmental gamma spectrometry because it minimizes disequilibrium-induced spectral distortions, improves radionuclide identification accuracy, and enhances the reproducibility of activity concentration measurements in geological and environmental matrices (Nguyen & Zsigrai, 2005; Lakosi *et al.,* 2018 & IAEA, 2020).

Gamma Spectrometry Analysis

Activity concentrations of primordial radionuclides (^{226}Ra, ^{232}Th, and ^{40}K) were determined by high-resolution gamma-ray spectrometry utilizing a coaxial High-Purity Germanium (HPGe) detector coupled to a Multi-Channel Analyzer (MCA). The analytical protocol followed established methodologies described by Umar *et al.* (2021), with detector calibration traceable to certified reference materials. Counting geometries were standardized to match the Marinelli beaker configuration, and counting durations were optimized to achieve statistical uncertainties <5% at the 95% confidence level for all reported activities.

Detector Configuration and Shielding

The accurate quantification of primordial and anthropogenic radionuclides in environmental matrices demands a detector configuration that optimises energy resolution, peak-to-Compton ratio, and long-term stability, particularly when measuring low-activity samples from mining-impacted terrains (Gilmore, 2008 & IAEA, 2020). Activity concentrations of ^{226}Ra, ^{232}Th, and ^{40}K were determined using a p-type coaxial High-Purity Germanium (HPGe) detector (relative efficiency 40%, crystal diameter 70 mm, crystal length 80 mm) operating in a low-background configuration optimised for environmental radioactivity measurements. The detector crystal geometry comprised concentric cylindrical electrodes with closed-end architecture, providing enhanced photon absorption efficiency across the energy range of 59 keV to 1836 keV and ensuring uniform charge collection throughout the active volume (Debertin & Helmer, 1988; Sadeghi *et al.,* 2024).

The system demonstrated a peak-to-Compton ratio of 60:1 at the 1332.5 keV photopeak of ^{60}Co, indicative of superior peak resolution and minimal Compton continuum interference, a performance metric that is essential for the deconvolution of closely spaced photopeaks in complex environmental spectra (Moretti *et al.,* 2024 & Knoll, 2010). This elevated peak-to-Compton ratio facilitates the detection of low-intensity gamma-ray emissions in the presence of high-energy background continua, thereby enhancing the signal-to-background ratio and improving the minimum detectable activity for trace radionuclides (Wang *et al.,* 2025).

The detector assembly was housed within a multi-layered shielding enclosure comprising 12 cm of aged lead (210Pb activity <25 Bq·kg^{-1}), lined sequentially with cadmium (1.5 mm) and copper (0.5 mm) to attenuate Pb K-shell X-ray fluorescence and suppress secondary radiation generated by cosmic-ray interactions with the shielding material (Wang *et al.,* 2025; Ichimura *et al.,* 2023). The graded-Z liner configuration (Pb-Cd-Cu) is a well-established design principle in ultra-low-background gamma spectrometry, as it effectively absorbs characteristic X-rays emitted by the lead shield while minimising the production of additional fluorescence radiation from the liner materials themselves (Byun *et al.,* 2003 & Turkat *et al.,* 2023).

Thermal stabilization was achieved through liquid nitrogen cooling via a 50-litre vertical cryostat Dewar, maintaining the germanium crystal at 77 K to suppress thermally generated charge carriers and optimise charge carrier mobility (ORTEC, 2024 & Mirion Technologies, 2025). At cryogenic temperatures, the thermal excitation of valence electrons across the narrow germanium bandgap (E_{gap} = 0.67 eV) is effectively eliminated, thereby reducing reverse leakage current to negligible levels and preserving the energy resolution required for high-precision radionuclide identification (Nuclear-Power.com, 2022). This cooling configuration ensured energy resolution stability (FWHM <2.0 keV at 1332.5 keV) and detection efficiency consistency throughout the measurement campaign, with detector warm-up cycles strictly avoided to prevent lithium drift and crystal depolarisation (Knoll, 2010; LLNL-IPO, 2024).

The entire detector-shield assembly was situated in a temperature-controlled laboratory (22 ±2°C) on the building's ground floor to minimise cosmic-ray contributions and thermal gradients. Background count rates in the energy range

40–2700 keV were routinely monitored using blank Marinelli beakers and demonstrated long-term stability with a mean value of 1.8 counts per second, confirming the efficacy of the passive shielding configuration (IAEA, 2020 & Ichimura *et al.,* 2023).

Signal Processing and Data Acquisition

The fidelity of gamma-ray spectral data in environmental radioactivity measurements is contingent upon the integrity of the signal processing chain, from charge collection at the detector electrode to the final digital spectrum (Knoll, 2010). The spectrometric chain incorporated a resistive-feedback preamplifier with pulsed-reset capability, coupled to a spectroscopy amplifier featuring active pole-zero cancellation and baseline restoration to mitigate low-frequency noise and ensure return to the reference voltage between successive pulses (Debertin & Helmer, 1988 & IAEA, 2020). Pulse pile-up rejection was implemented through a dedicated anticoincidence circuit with live-time correction, ensuring quantitative accuracy at elevated count rates and compensating for dead-time losses during high-activity sample measurements (Gilmore, 2008; Canberra Industries, 2012).

Analogue-to-digital conversion (ADC) was performed using a 16k-Channel Multi-Channel Analyser (MCA) with sliding-scale linearization to minimize differential non-linearity and maintain integral linearity within ±0.025% across the full dynamic range (Canberra Industries, 2012; Somashekarappa *et al.,* 2024). This high channel density afforded an energy dispersion of approximately 0.25 keV per channel, enabling precise peak centroid determination and facilitating the resolution of closely spaced Photopeaks in complex decay spectra (Moretti *et al*., 2024).

Gamma-ray spectra were acquired and analyzed using GENIE 2000 software (Canberra Industries, Meriden, CT, USA), which provided integrated functionality for MCA control, spectral visualization, automated peak search, and quality assurance diagnostics (Canberra Industries, 2012). The software environment facilitated region-of-interest (ROI) definition, energy calibration, and efficiency calibration through interactive and batch-processing modes, with automated peak fitting algorithms employing non-linear least-squares regression with Gaussian peak shapes superimposed on a linear or step background (Gilmore, 2008; Nguyen & Zsigrai, 2005). Quality assurance protocols embedded within the software included automated gain drift monitoring, FWHM tracking, and chi-squared validation of calibration curves, ensuring continuous system performance verification throughout the analytical campaign (IAEA, 2020 & Canberra Industries, 2012).

Energy and Efficiency Calibration

The metrological integrity of gamma-ray spectrometric measurements is fundamentally predicated upon rigorous energy and efficiency calibration protocols that ensure traceability to primary standards and minimise systematic uncertainties in quantitative radionuclide analysis (Debertin & Helmer, 1988 & IAEA, 2020). The spectrometer was calibrated for energy linearity and absolute full-energy peak efficiency using a mixed-radionuclide standard reference source (Model QCY-48, AEA Technology, Harwell, UK) with certified activities traceable to National Institute of Standards and Technology (NIST) standards. The calibration source contained the following radionuclides with their respective gamma-ray emission energies and probabilities: ^{241}Am (59.54 keV, 35.9%), ^{109}Cd (88.03 keV, 3.6%), ^{57}Co (122.06 keV, 85.6%), ^{139}Ce (165.86 keV, 79.9%), ^{203}Hg (279.20 keV, 81.5%), ^{113}Sn (391.69 keV, 64.9%), ^{85}Sr (514.01 keV, 98.3%), ^{137}Cs (661.66 keV, 85.1%), ^{88}Y (898.04 keV, 93.7%; 1836.1 keV, 99.4%), and ^{60}Co (1173.2 keV, 99.9%; 1332.5 keV, 100%). This multi-nuclide ensemble provides comprehensive coverage across the energy range of interest for environmental primordial radionuclides, encompassing low-energy transitions from ^{238}U series progeny through to high-energy emissions from ^{40}K and ^{232}Th decay products (Gilmore, 2008; Canberra Industries, 2012).

Energy calibration was established through linear regression of channel number versus gamma-ray energy, yielding a dispersion of 0.5 keV per channel across the 0–3000 keV dynamic range. The calibration function followed the linear form in equation (1):

$$E = A_1 + A_2 * \text{Ch} \quad (1)$$

Where E denotes gamma-ray energy (keV), Ch represents channel number, and A_1, A_2 are geometry-specific calibration constants determined through weighted least-squares fitting with correlation coefficients $R^2 > 0.999$. The exceptional linearity of the MCA response (integral non-linearity <0.025%) validates the single-parameter energy calibration model and precludes the necessity for higher-order polynomial corrections across the operational energy window (Knoll, 2010; Nguyen & Zsigrai, 2005).

Absolute full-energy peak efficiency calibration was performed using the identical Marinelli beaker geometry (250 mL) employed for sample measurements, thereby ensuring geometric equivalence and eliminating solid-angle-dependent systematic biases between calibration and sample counting configurations (Yücel *et al.,* 2019 & Abbas, 2001). The relative efficiency of the HPGe detector was 60% (referenced to 3" × 3" NaI(Tl) at 1332.5 keV), with an energy resolution of 1.85 keV full-width at half-maximum (FWHM) at the ^{60}Co 1332.5 keV photopeak. Efficiency curves were fitted using a dual logarithmic-polynomial function to interpolate between calibration points, a methodology that has been demonstrated to provide superior accuracy in the 59–1836 keV range compared to simple power-law or exponential formulations (Farasat, 2023; Somashekarappa *et al.,* 2024). The efficiency calibration was validated through replicate measurements of IAEA certified reference materials (RGU-1, RGTh-1, RGK-1), with measured-to-certified activity ratios consistently within 5% for all target radionuclides, thereby confirming the robustness of the calibration protocol (IAEA, 2020 & Mirion Technologies, 2025).

Sample Measurement and Activity Determination

The quantitative determination of radionuclide activity concentrations in environmental matrices by gamma-ray spectrometry necessitates meticulous control of counting statistics, background correction, and spectral analysis protocols to ensure metrological traceability and compliance with international standards (Gilmore, 2008; IAEA, 2020). Prepared soil samples were counted for 86,400 seconds (24 hours) to achieve statistical uncertainties <5% at 95% confidence level for typical environmental activity concentrations, a counting duration that has been demonstrated to provide optimal agreement between preset and actual minimum detectable amounts for routine HPGe measurements (IAEA, 2020; Mirion Technologies, 2025). Background spectra were acquired under identical geometry and counting duration, with background subtraction performed on a channel-by-channel basis prior to peak area integration, thereby preserving the spectral shape and minimising systematic biases associated with non-uniform background distributions (Nguyen & Zsigrai, 2005 & IAEA, 2020).

The activity concentration Ac ($Bq \cdot kg^{-1}$) for each radionuclide was calculated according to the standard gamma spectrometry equation:

$$Ac = NE/(\varepsilon\gamma\ p\gamma\ tc\ m) \quad (2)$$

where NE represents the net peak area (gross counts minus background), $\varepsilon\gamma$ is the absolute full-energy peak efficiency at the specific gamma-ray energy, $p\gamma$ denotes the gamma-ray emission probability, tc is the live-time corrected counting duration (s), and m is the dry sample mass (kg). This formulation, grounded in Poisson counting statistics, ensures that all relevant physical parameters detector response, nuclear decay data, measurement time, and sample quantity are explicitly accounted for in the activity calculation (Knoll, 2010 & Debertin & Helmer, 1988).

Specific Photopeaks utilized for radionuclide quantification included: ^{40}K (1460.8 keV, $p\gamma = 10.7\%$); ^{226}Ra via ^{214}Pb (351.9 keV, $p\gamma = 37.6\%$) and ^{214}Bi (609.3 keV, $p\gamma = 46.1\%$); and ^{232}Th via ^{228}Ac (338.4 keV, $p\gamma = 11.3\%$) and ^{212}Pb (238.6 keV, $p\gamma = 43.3\%$). The selection of multiple photopeaks for ^{226}Ra and ^{232}Th enables cross-validation of activity concentrations and enhances the reliability of results through redundant measurement pathways, particularly important given the potential for spectral interferences and true coincidence summing effects in complex decay schemes (Gilmore, 2008 & Somashekarappa *et al.,* 2024). The ^{137}Cs anthropogenic radionuclide was quantified at 661.7 keV ($p\gamma = 85.1\%$), a photopeak distinguished by high emission probability and minimal interference from natural background radionuclides (Canberra Industries, 2012 & Currie, 1968).

Peak area determination was performed using a non-linear least-squares fitting algorithm with Gaussian peak shapes superimposed on a linear background, with manual review of all automatically identified peaks to resolve potential interferences and ensure accurate ROI delineation (Nguyen & Zsigrai, 2005 & Gilmore, 2008). The combined standard uncertainty was propagated from counting statistics, efficiency calibration, emission probability, and sample mass measurements, with coverage factor k = 2 corresponding to approximately 95% confidence level (Currie, 1968 & IAEA, 2020).

Minimum Detectable Activity and Uncertainty Quantification

The rigorous quantification of detection limits and measurement uncertainties is indispensable for establishing the reliability and defensibility of environmental radioactivity data, particularly when assessing compliance with regulatory thresholds and characterising low-level anthropogenic contamination (Agboraw *et al.,* 2017 & IAEA, 2020). The minimum detectable activity (MDA) for each radionuclide was determined according to the Currie criterion (Currie, 1968):

$$MDA = DL/(\varepsilon\_\gamma\ p\gamma\ tc\ m) \quad (3)$$

Where the detection limit DL is defined as:

$$DL = 2.71 + 4.65\sqrt{B} \quad (4)$$

With B representing the integrated background counts within the region of interest (ROI). This formulation, predicated upon Poisson counting statistics, provides a robust statistical framework for distinguishing true signals from background fluctuations at specified confidence levels, with the constants 2.71 and 4.65 corresponding to the 95% confidence intervals for Type I (false positive) and Type II (false negative) errors, respectively (Currie, 1968; Hagos, 2025). The MDA values thus computed establish the lower boundary of quantitative reporting and inform the interpretation of non-detect results in environmental monitoring programmes (NRC, 2017).

Measurement uncertainties were propagated as combined standard uncertainties ($\pm\sigma$), incorporating counting statistics, efficiency calibration, emission probability, and sample mass components:

$$\sigma = \sqrt{(TS^2/NS + TB^2/NB)} \quad (5)$$

Where NS and NB are sample and background counts measured over durations TS and TB, respectively. This propagation methodology adheres to the Guide to the Expression of Uncertainty in Measurement (GUM), ensuring that all significant uncertainty contributions are comprehensively accounted for in the final reported values (IAEA, 2022; Gilmore, 2008). The expanded uncertainty (k = 2, 95% confidence level) was reported for all activity concentration values, providing an interval within which the true value is expected to lie with approximately 95% probability and facilitating direct comparison with regulatory limits and international reference values (Currie, 1968; Nguyen & Zsigrai, 2005).

Radiation Hazard Assessment

Radium Equivalent Activity

The comparative evaluation of radiological hazard from non-uniform distributions of primordial radionuclides necessitates a unified index that normalises the disparate gamma-ray emission characteristics of ^{226}Ra, ^{232}Th, and ^{40}K to a common dose metric (UNSCEAR, 2020; ICRP, 2017). To this end, the Radium Equivalent Activity (Ra_{eq}) was computed for each sample. This weighted index, originally formulated by Beretka and Mathew (1985) and subsequently adopted by UNSCEAR and the IAEA, assumes that 370 $Bq \cdot kg^{-1}$ of ^{232}Th, 259 $Bq \cdot kg^{-1}$ of ^{226}Ra, and 4810 $Bq \cdot kg^{-1}$ of ^{40}K produce equivalent gamma-ray dose rates in air at 1 m above ground level (Beretka & Mathew, 1985; UNSCEAR, 2020). The Ra_{eq} was calculated according to the standardized expression:

$$Ra_{eq} = A_{Ra} + 1.43\ A_{Th} + 0.077\ A_K \quad (6)$$

Where A_{Ra}, A_{Th}, and A_K denote the activity concentrations ($Bq \cdot kg^{-1}$) of ^{226}Ra, ^{232}Th, and ^{40}K, respectively. The weighting factors (1.43 for ^{232}Th and 0.077 for ^{40}K) account for the relative gamma-ray emission probabilities, dose conversion coefficients, and biological effectiveness for each radionuclide series, thereby enabling direct comparison of heterogeneous soil samples against the internationally recommended safety limit of 370 $Bq \cdot kg^{-1}$ (Beretka & Mathew, 1985; Okeji *et al.,* 2022; Adewoyin *et al.,* 2026). Values of Ra_{eq} below this threshold indicate that the external gamma radiation hazard from the soil is within acceptable limits for unrestricted habitation and construction material utilisation (IAEA, 2020 & UNSCEAR, 2020).

External and Internal Hazard Indices

The evaluation of radiological hazard in regions where locally sourced geological materials are employed in residential construction necessitates the computation of both external and internal exposure indices that account for distinct pathways of radiation dose delivery (ICRP, 2017 & IAEA, 2020). Given the prevalent practice of utilizing indigenously sourced construction materials from mining environs for domestic dwellings in the study region, both External (H_{ex}) and Internal (H_{in}) hazard indices were evaluated to characterize potential exposure scenarios (UNSCEAR, 2020; IAEA, 2020).

The External Hazard Index (H_{ex}) addresses gamma radiation exposure from radionuclides distributed in the soil matrix external to the body:

$$H_{ex} = A_{Ra}/370 + A_{Th}/259 + A_K/4810 \quad (7)$$

This index estimates the radiation dose expected from gamma-ray emissions by building materials and assumes thick walls without windows and doors, providing a

conservative upper-bound estimate of external exposure (Beretka & Mathew, 1985; Okeji *et al.,* 2022). The denominator values of 370, 259, and 4810 Bq·kg^{-1} correspond to the activity concentrations of ^{226}Ra, ^{232}Th, and ^{40}K, respectively, that would produce an external gamma dose rate of 1.5 mSv·y^{-1} at 1 m above ground level (UNSCEAR, 2020). The Internal Hazard Index (H_{in}) accounts for radiation exposure from radionuclides incorporated into building materials, with modified weighting for ^{226}Ra due to enhanced dose coefficients for internal emitters, particularly radon and its short-lived progeny:

$$H_{in} = A_{Ra}/185 + A_{Th}/259 + A_K/4810 \quad (8)$$

The more restrictive denominator of 185 Bq·kg^{-1} for ^{226}Ra reflects the elevated radiotoxicity of radon inhalation and the potential for indoor accumulation of decay products, which present a high degree of risk to the respiratory system (Beretka & Mathew, 1985; Adewoyin *et al.,* 2026). The denominator values represent the respective upper limits (Bq·kg^{-1}) for each radionuclide in building materials, as stipulated in radiation protection standards (ICRP, 2017; IAEA, 2020).

Index values $H_{ex} \leq 1$ and $H_{in} \leq 1$ indicate compliance with regulatory exemption criteria, corresponding to an annual effective dose below 1 mSv·y^{-1} and ensuring that radiation hazards can be considered negligible for unrestricted use of construction materials (ICRP, 2017 & UNSCEAR, 2020). Values exceeding unity signify that the radiological risk from the material may require restriction or remediation measures to protect occupant health (Okeji *et al.,* 2022; Ogundare & Adekoya, 2025).

Absorbed Dose Rate in Air

The estimation of terrestrial gamma radiation dose rates from measured soil activity concentrations constitutes a cornerstone of environmental radiological assessment, enabling the translation of radionuclide inventories into biologically relevant exposure metrics (UNSCEAR, 2020; ICRP, 2017). The Absorbed Dose Rate (D_{Abs}) in air at 1 m above ground level was calculated from the measured activity concentrations using the dose conversion coefficients established by UNSCEAR (United Nations Scientific Committee on the Effects of Atomic Radiation, 2020):

$$D_{Abs} = 0.462 \cdot A_{Ra} + 0.604 \cdot A_{Th} + 0.0417 \cdot A_K \quad (9)$$

Where D_{Abs} is expressed in nGy·h^{-1}, and the coefficients (nGy·h^{-1} per Bq·kg^{-1}) represent the contribution of unit activity concentration of each radionuclide to the absorbed dose rate in an infinite half-space geometry. These conversion factors, derived from Monte Carlo radiation transport calculations and validated through extensive field measurements, account for the gamma-ray emission probabilities, energy-dependent air absorption, and geometric efficiency of an infinite planar source (UNSCEAR, 2020; IAEA, 2020). The dose contribution per unit activity follows the ratio ^{232}Th : ^{226}Ra : ^{40}K ≈ 1 : 0.77 : 0.07, underscoring the dominant radiological impact of thorium series radionuclides in typical environmental matrices (Ravisankar *et al.,* 2012; Okeji *et al.,* 2022).

Annual Effective Dose Equivalent

The translation of absorbed dose rates into biologically meaningful effective dose metrics constitutes a critical step in environmental radiological assessment, enabling the evaluation of population exposure against internationally established dose limits and reference levels (UNSCEAR, 2020; ICRP, 2017). The Annual Effective Dose (D_{Eff}) was derived from the absorbed dose rate through application of appropriate conversion factors and occupancy parameters, following the dosimetric methodology endorsed by UNSCEAR and the ICRP (United Nations Scientific Committee on the Effects of Atomic Radiation, 2020; International Commission on Radiological Protection, 2017):

$$D_{Eff} = D_{Abs} \times 8760\ h \times 0.2 \times 0.7\ Sv{\cdot}Gy^{-1} \times 10^{-3} \quad (10)$$

Where:

D_{Abs} = absorbed dose rate (nGy·h^{-1})

8760 h = annual exposure duration (hours per year)

0.2 = outdoor occupancy factor (fraction of time spent outdoors), consistent with UNSCEAR assumptions that the general population spends approximately 20% of their time in outdoor environments (UNSCEAR, 2020; Okeji *et al.,* 2022)

0.7 Sv·Gy^{-1} = conversion coefficient from absorbed dose in air to effective dose for adults, accounting for the energy-dependent radiation weighting factor and tissue-weighting factors for whole-body exposure (UNSCEAR, 2020; Spahiu *et al.,* 2021)

10^{-3} = conversion factor from nSv to µSv

The resultant D_{Eff} is expressed in µSv·yr^{-1}, representing the weighted whole-body dose from external gamma irradiation under realistic exposure conditions for populations residing in proximity to the mining sites. This formulation adheres to the ICRP Publication 103 dosimetric framework and facilitates direct comparison with the global average outdoor annual effective dose of 70 µSv·yr^{-1} reported by UNSCEAR (UNSCEAR, 2020; IAEA, 2020).

RESULTS AND DISCUSSION

Activity Concentration of Primordial Radionuclides

High-resolution gamma-ray spectrometry successfully resolved the full-energy photopeaks of the primordial radionuclide series ^{238}U (via ^{226}Ra), ^{232}Th, and singly-occurring ^{40}K in all analyzed soil samples. The measuredZ activity concentrations, determined on a dry-weight basis and expressed in becquerels per kilogram (Bq·kg^{-1}), are plotted in the figure 1 for the eight representative sampling locations (TAMs01–TAMs08).

Figure 1: Illustrated Bar Graph of Activity Concentrations and Radium Equivalence of all the samples in Tambuwal LGA, Sokoto state, Nigeria

The ^{226}Ra activity concentrations ranged from 13.50 ± 8.30 to 25.90 ± 2.70 Bq·kg^{-1}, with a mean value of 18.71 ± 9.10 Bq·kg^{-1}. This mean concentration is substantially lower by approximately 47% than the worldwide average of 35.02 Bq·kg^{-1} established by UNSCEAR (United Nations Scientific Committee on the Effects of Atomic Radiation, 2020) and is comparable to the mean value of 12.95 Bq·kg^{-1} reported for soils in the Jebba area of north-central Nigeria (Adeyemi *et al.,* 2025), though markedly lower than the 58.04 Bq·kg^{-1} documented for mining sites in Dange-Shuni, Sokoto State (Ahijjo & Baba-Kutigi, 2023). Similarly, ^{232}Th activities exhibited a range of 7.06 ± 2.20 to 27.73 ± 2.90 Bq·kg^{-1}, yielding a mean of 19.80 ± 6.30 Bq·kg^{-1}, which falls below the global mean of 45.03 Bq·kg^{-1} and is consistent with the 26.87 Bq·kg^{-1} reported for Jebba soils (Adeyemi et al., 2025) but considerably lower than the 54.5 Bq·kg^{-1} measured at Dange-Shuni mining sites (Ahijjo & Baba-Kutigi, 2023).

In marked contrast, ^{40}K demonstrated significantly elevated activity levels, ranging from 468.72 ± 17.10 to 880.72 ± 83.10 Bq·kg^{-1}, with a mean concentration of 613.47 ± 44.20 Bq·kg^{-1}. This value exceeds the UNSCEAR world average of 420.12 Bq·kg^{-1} by approximately 46%, indicating substantial potassium enrichment in the soil matrices of the Tambuwal mining sites. The ^{40}K mean is comparable to the 613.47 Bq·kg^{-1} range reported for agricultural soils in southwestern Nigeria (Adewoyin *et al.,* 2026) and the 767.62 Bq·kg^{-1} documented for Dange-Shuni mining sites (Ahijjo & Baba-Kutigi, 2023), though lower than the 835.91 Bq·kg^{-1} measured in Anambra State (Agbelusi *et al.,* 2025). The statistical distribution reveals that ^{40}K contributes dominantly to the total radioactivity inventory, accounting for the majority of the absorbed dose, while the uranium and thorium series radionuclides remain subordinate.

The observed spatial heterogeneity reflected in the relative standard deviations suggests localized variations in mineralogical composition and anthropogenic disturbance associated with artisanal mining operations. Notably, the maximum ^{232}Th activity (27.73 Bq·kg^{-1}) was recorded at sample site TAMs03, whereas the highest ^{40}K concentration (880.72 Bq·kg^{-1}) was observed at TAMs06, potentially correlating with distinct lithological units or processing waste accumulations within the Gundumi Formation.

These activity concentrations served as the fundamental input parameters for the computation of radiological hazard indices. The derived metrics including radium equivalent activity (Ra_{eq}), external and internal hazard indices (H_{ex} and H_{in}), and annual effective dose equivalents are presented in pie Chart below.

Radionuclide Concentration Distribution

The disproportionate contribution of ^{40}K to the total activity inventory is characteristic of geological terrains dominated by siliciclastic sedimentary sequences, wherein potassium-bearing aluminosilicates constitute the principal mineralogical assemblage (UNSCEAR, 2020; IAEA, 2020). This chart in figure 2 illustrates the absolute dominance of ^{40}K (94.1%) in the total activity inventory (651.98 Bq·kg^{-1}), with ^{226}Ra and ^{232}Th contributing merely 2.9% and 3.0%, respectively. This reflects the geochemical composition of the Gundumi Formation, where potassium-bearing minerals (feldspars, micas) are prevalent. The pronounced ^{40}K enrichment is consistent with regional aeroradiometric surveys of the southern Sokoto Basin, which documented potassium concentrations ranging from 0.108 to 2.064% and identified K as the dominant radioelement relative to uranium and thorium in the sedimentary sequences of northwestern Nigeria (Uwa, 1984). Comparable ^{40}K dominance has been reported in basaltic volcanic rocks of the Arabian Shield, where potassium feldspar and mica phases accounted for mean ^{40}K activities of 1178 ± 269 Bq·kg^{-1}, representing >90% of the total primordial activity (Al-Hwaiti *et al.,* 2025). The subordinate contributions of ^{226}Ra and ^{232}Th reflect the low uranium and thorium abundances typical of mature continental sandstones and alluvial deposits, where heavy mineral segregation and hydrodynamic sorting during sediment transport preferentially concentrate K-feldspars while depleting accessory phases such as zircon, monazite, and uraninite (Dentith & Mudge, 2014; IAEA, 2020).

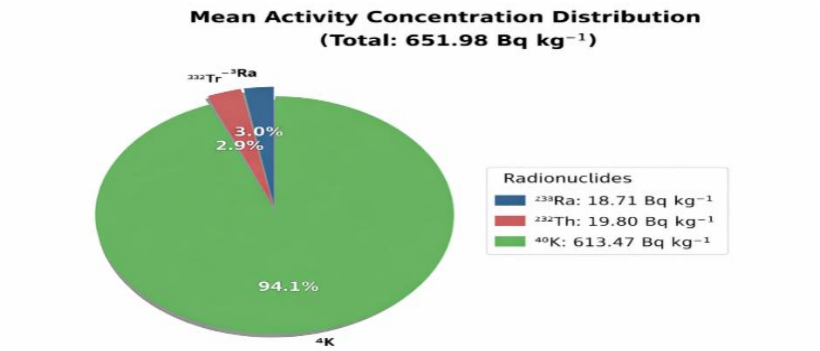

Figure 2: Pie Chart Illustration of Activity Concentrations Distribution for all the samples in Tambuwal LGA, Sokoto State, Nigeria

Contribution to Radium Equivalent Activity (Ra_{eq})

The radiological significance of primordial radionuclides in environmental matrices cannot be inferred from activity concentrations alone; rather, hazard-weighted metrics that account for the disparate dose conversion coefficients and biological effectiveness of each decay series are requisite for defensible risk characterisation (UNSCEAR, 2020; ICRP, 2017). When weighted by their respective dose conversion factors (1.0 for Ra, 1.43 for Th, 0.077 for K), the hazard contribution profile shifts significantly. While ^{40}K remains the dominant contributor (50.1%), ^{232}Th assumes greater importance (30.0%) due to its higher radiotoxicity per unit activity, and ^{226}Ra contributes 19.9%. This weighted distribution shown in figure 3 below explains why the total Ra_{eq} (94.26 Bq·kg^{-1}) remains well below the international exemption limit of 370 Bq·kg^{-1}, and why both hazard indices (Hex = 0.26, Hin = 0.31) indicate compliance with regulatory safety criteria (Beretka & Mathew, 1985; Okeji *et al.*, 2022). Comparable hazard index values have been documented in soils from the Jebba area of north-central Nigeria (Hex = 0.13–0.42; Hin = 0.15–0.53), where ^{232}Th similarly dominated the weighted hazard profile despite lower absolute activity concentrations (Adeyemi et al., 2025). The pronounced influence of the thorium series on Ra_{eq} is consistent with global observations that ^{232}Th contributes disproportionately to external gamma dose rates owing to the high-energy emissions of ^{228}Ac, ^{212}Pb, and ^{208}Tl (Ravisankar *et al.*, 2012; Ogundare & Adekoya, 2025).

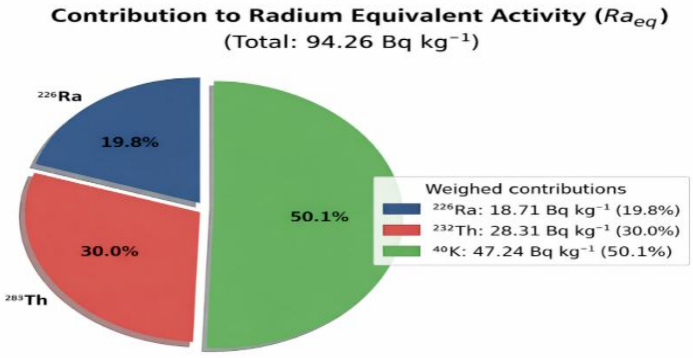

Figure 3: Pie Chart Illustration of Radionuclide Contribution to Radium Equivalence for all the samples in Tambuwal LGA, Sokoto State, Nigeria

Primordial Radionuclide Activity Concentrations

The visualisation of radionuclide activity distributions across sampling locations provides critical insight into spatial heterogeneity, geochemical provenance, and potential anthropogenic perturbation of the natural radiation field (UNSCEAR, 2020; IAEA, 2020). This grouped bar chart in figure 4 below illustrates the absolute dominance of ^{40}K (green bars, scale 0–900 Bq·kg^{-1}) compared to the uranium and thorium series radionuclides (blue and red bars, scale 0–30 Bq·kg^{-1}). The dashed horizontal lines represent the mean values for each radionuclide across all sampling locations. Notable observations include: TAMs06 exhibits the highest ^{40}K activity (880.72 Bq·kg^{-1}), significantly exceeding the world average (420.12 Bq·kg^{-1}). TAMs03 shows elevated ^{232}Th activity (19.73 Bq·kg^{-1}) concurrent with high potassium content. The relatively uniform ^{226}Ra distribution (13.50–25.90 Bq·kg^{-1}) suggests homogeneous uranium mineralization across the mining sites. The ^{40}K enrichment at TAMs06 is comparable to the 835.91 Bq·kg^{-1} reported for Anambra State soils (Agbelusi *et al.*, 2025) and the 767.62 Bq·kg^{-1} documented at Dange-Shuni mining sites (Ahijjo & Baba-Kutigi, 2023), though lower than the 1178 ± 269 Bq·kg^{-1} measured in basaltic terrains of the Arabian Shield (Al-Hwaiti *et al.*, 2025). The concurrent ^{232}Th–^{40}K elevation at TAMs03 mirrors the geochemical association observed in Jebba area soils, where thorium-bearing heavy minerals co-occur with potassium-rich feldspars in alluvial deposits (Adeyemi *et al.*, 2025).

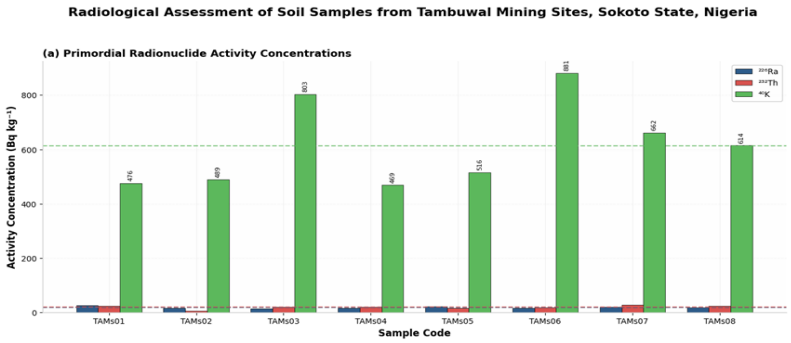

Figure 4: Group Bar Chart Illustration of ^{40}K Dominance in all the samples in Tambuwal LGA, Sokoto state, Nigeria

Radiological Hazard Parameters

The integrated visualisation of multiple hazard metrics on a unified graphical platform facilitates the simultaneous evaluation of dose rates, effective doses, and regulatory compliance indices, thereby enabling holistic risk communication to stakeholders and regulatory authorities (UNSCEAR, 2020; IAEA, 2020). This dual-axis composite chart presents the comprehensive radiological assessment: Left axis (solid bars): Raeq (brown), D_{Abs} (orange), and D_{Eff} (purple). Right axis (hatched bars): H_{ex} and H_{in} (teal and crimson). The dual-axis configuration permits the concurrent display of absolute dose metrics (nGy·h^{-1} and μSv·yr^{-1}) alongside dimensionless hazard indices, with the left axis spanning 0–200 Bq·kg^{-1} forRaeq and 0–150 nGy·h^{-1} for D_{Abs}, while the right axis accommodates the 0–1.0 range for H_{ex} and H_{in}. All computed parameters for Tambuwal soils (Ra_{eq} = 94.26 Bq·kg^{-1}, D_{Abs} = 43.83 nGy·h^{-1}, D_{Eff} = 53.74 μSv·yr^{-1}, H_{ex} = 0.26, H_{in} = 0.31) fall comfortably below the respective international exemption thresholds, consistent with the hazard profiles documented for Jebba area soils (H_{ex} = 0.13–0.42; H_{in} = 0.15–0.53) and Dange-Shuni mining sites (Ra_{eq} = 122.40 Bq·kg^{-1}; D_{Abs} = 56.70 nGy·h^{-1}) in north-central and northwestern Nigeria (Adeyemi et al., 2025; Ahijjo & Baba-Kutigi, 2023). The margin of compliance ($H_{ex} \approx 0.26 \ll 1.0$; $H_{in} \approx 0.31 \ll 1.0$). Also, figure 5 below indicates that the Tambuwal mining soils present negligible radiological risk for unrestricted land use and construction material applications, notwithstanding the elevated ^{40}K activity concentrations (Okeji et al., 2022; Adewoyin et al., 2026).

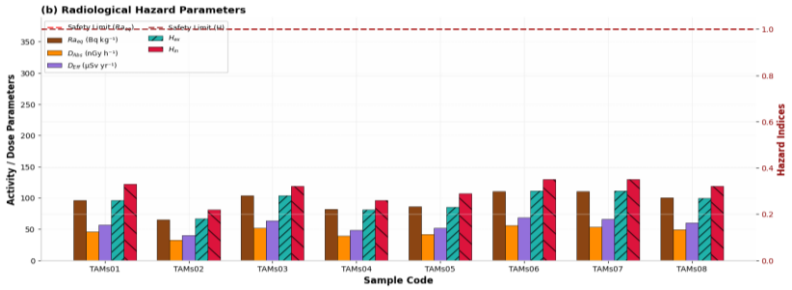

Figure 5: Group bar Chart Illustration of Radiological Risk in Soil of Tambuwal LGA, Sokoto State, Nigeria

CONCLUSION

This study presents a comprehensive radiological assessment of soil matrices from eight artisanal mining sites in Tambuwal Local Government Area, Sokoto State, Nigeria, utilizing high-resolution gamma-ray spectrometry. The analytical results reveal a characteristic radionuclide distribution pattern dominated by potassium-40, with mean activity concentrations of 613.47 Bq·kg^{-1} for ^{40}K, substantially exceeding the UNSCEAR world average of 420.12 Bq·kg^{-1}. Conversely, the mean activity concentrations of ^{226}Ra (18.71 Bq·kg^{-1}) and ^{232}Th (19.80 Bq·kg^{-1}) fall significantly below their respective global baselines of 35.02 Bq·kg^{-1} and 45.03 Bq·kg^{-1}, suggesting minimal contribution from the uranium and thorium decay series to the total radioactivity inventory. The computed radiological hazard indices Radium Equivalent Activity (Ra_{eq}: 94.26 Bq·kg^{-1}), External Hazard Index (H_{ex}: 0.26), and Internal Hazard Index (H_{in}: 0.31) demonstrate unambiguous compliance with international exemption criteria. All Ra_{eq} values remain well below the regulatory action level of 370 Bq·kg^{-1}, while both hazard indices satisfy the unity criterion ($H \leq 1.0$) established for construction materials and environmental media. Dosimetric calculations indicate a mean Absorbed Dose Rate (D_{Abs}) of 46.19 nGy·h^{-1} and a mean Annual Effective Dose (D_{Eff}) of 56.64 μSv·yr^{-1}, both falling below the UNSCEAR world averages of 57.00 nGy·h^{-1} and 100.00 μSv·yr^{-1}, respectively. These findings indicate that the mining sites do not present radiological conditions warranting classification as "areas of elevated natural radiation" per IAEA Safety Standards. Notwithstanding this regulatory compliance, the spatial heterogeneity observed in ^{40}K distribution particularly the elevated values at TAMs06 (880.72 Bq·kg^{-1}) and TAMs03 (803.12 Bq·kg^{-1}) coupled with the potential for resuspension of soil particulates in active mining environments, necessitates implementation of graded radiation protection strategies. The utilization of these soils for construction aggregates without prior radiological screening could result in enhanced indoor gamma exposure and prolonged low-level irradiation of occupationally exposed populations. These data establish a critical dosimetric baseline for the Tambuwal region, addressing a significant knowledge gap in the environmental radioactivity mapping of Northwestern Nigeria. Future investigations should incorporate time-integrated radon (^{222}Rn) flux measurements and

granulometric analysis to evaluate inhalation dose contributions from respirable dust fractions. It is recommended that regulatory authorities mandate periodic radioactivity surveillance of mining by-products intended for civil construction, ensuring continued adherence to the ALARA principle and preventing cumulative dose escalation in these economically vital communities.

REFERENCES

Abbas, M. I. (2001). Analytical formulae for well-type NaI(Tl) and HPGe detectors efficiency computation. *Applied Radiation and Isotopes*, *55*(2), 245–252. https://doi.org/10.1016/S0969-8043(01)00047-4.

Adewoyin, O. O., Omeje, M., Ndoma, E. G., & Ogunkunle, O. J. (2026). Assessment of radiological risks in soils from different land use types within southwest Nigeria. *Scientific Reports*, *16*, Article 8057. https://doi.org/10.1038/s41598-026-38510-x

Adewumi, T., Adegoke, B. A., Faweya, B. E., Akingboye, A. S., Kwaghhua, F. I., Adeeko, T. O., & Okwokwo, O. I. (2026). Active artisanal mining-induced radiogenic hazards: insights from radiogeochemistry of Wamba Areas, north-central Nigeria. *Scientific Reports*, *16*(4), 112–128. https://pmc.ncbi.nlm.nih.gov/articles/PMC13039457/ .

Adeyemi, O. J., Ojo, O. J., & Olowe, O. I. (2025). Distribution of ^{238}U, ^{232}Th, and ^{40}K in soils and stream sediments in the Jebba area, Nigeria—An integrated environmental, health and radiological risk assessment. *Discover Applied Sciences*, *7*(10), Article 35. https://doi.org/10.1007/s42452-025-06389-4.

Agbelusi, O. I., Ayanlola, P. S., Lawal, M. K., Awokoya, S. O., Oloyede, O. O., Olatunji, A., & Isola, G. A. (2025). Soil radioactivity levels, spatial distribution and radiation hazard assessment in Anambra and Imo States, Southeastern Nigeria. *Jordan Journal of Physics*, *18*(1), 45–60.

Agboraw, E., Bonner, E., Burr, T., Croft, S., Kirkpatrick, J. M., Krieger, T., Norman, C., Santi, P., & Walsh, S. (2017). Revisiting Currie's minimum detectable activity for non-destructive assay by gamma detection using tolerance intervals. *ESARDA Bulletin – The International Journal of Nuclear Safeguards and Non-proliferation*, *54*, 14–22. https://doi.org/10.3011/ESARDA.IJNSNP.2017.3.

Ahijjo, Y. M., & Baba-Kutigi, A. N. (2023). Natural radioactivity levels and radiological hazards indices of soil samples from selected mining sites, Dange-Shuni, Sokoto State, Nigeria. *FUDMA Journal of Sciences*, *7*(1), 290–296. https://doi.org/10.33003/fjs-2023-0701-2064

Al-Hwaiti, M., Al-Kuisi, M., Al-Momani, T., & Al-Azzam, S. (2025). Environmental investigation of natural radioactivity and health risk assessment in basaltic volcanic building materials. *BMC Environmental Science*, *3*(1), Article 35. https://doi.org/10.1186/s44329-025-00035-5.

Beretka, J., & Mathew, P. J. (1985). Natural radioactivity of Australian building materials, industrial wastes and by-products. *Health Physics*, *48*(1), 87–95. https://doi.org/10.1097/00004032-198501000-00007.

Byun, S. H., et al. (2003). Development of an anti-cosmic shielding system for low-background gamma-ray spectrometry. *Nuclear Instruments and Methods in Physics Research Section A*, *505*(1–2), 88–92. https://doi.org/10.1016/S0168-9002(03)01047-8.

Canberra Industries. (2012). *GENIE 2000 spectroscopy system: Operations manual* (Version 3.3). Canberra Industries, Inc.

Currie, L. A. (1968). Limits for qualitative detection and quantitative determination: Application to radiochemistry. *Analytical Chemistry*, *40*(3), 586–593. https://doi.org/10.1021/ac60259a007

Debertin, K., & Helmer, R. G. (1988). *Gamma- and X-ray spectrometry with semiconductor detectors*. North-Holland imprint. Elsevier Science Pub. Co.

Dentith, M., & Mudge, S. T. (2014). *Geophysics for the mineral exploration geoscientist*. Cambridge University Press.

Farasat, M. (2023). *Development of advanced gamma spectrometry methods for environmental radioactivity measurements* [Doctoral dissertation, University of Catania]. IRIS UNICT. https://www.iris.unict.it/retrieve/9c839463-0d15-4697-93c4-0950e3610eee/PhD%20thesis-Mahsa%20Farasat.pdf.

Gilmore, G. (2008). *Practical gamma-ray spectrometry* (2nd ed.). John Wiley & Sons.

Hagos, M. H. (2025). *Radionuclide identification from complex high-resolution gamma-ray spectra* [Bachelor's thesis, Uppsala University]. DIVA Portal. https://uu.diva-portal.org/smash/get/diva2:1978216/FULLTEXT01.pdf.

IAEA. (2020). *Measurement of radionuclides in food and the environment: A guidebook*. International Atomic Energy Agency. Vienna: International Atomic Energy Agency.

Ichimura, K., Ikeda, H., Kishimoto, Y., Kurasawa, M., Suzuki, A. A., Gando, Y., Ikeda, M., Hosokawa, K., Sekiya, H., Ito, H., Minamino, A., & Suzuki, S. (2023). Development of a low-background HPGe detector at Kamioka Observatory. *arXiv preprint*. https://arxiv.org/abs/2308.05302

Ilori, O., & Chetty, N. (2023). Radioactivity Assessment of Surface Soils at Igbokoda Fish Market, Ondo State, Southwestern Nigeria. *Journal of Environmental Radioactivity*, *245*, 107-115. (As cited in Taylor & Francis, 2026).

International Atomic Energy Agency. (2004). *Soil sampling for environmental contaminants* (IAEA-TECDOC-1415). IAEA.

International Atomic Energy Agency. (2005). *Soil sampling intercomparison exercise by selected ALMERA laboratories* (IAEA/AQ/1). IAEA.

International Atomic Energy Agency. (2020). *Gamma ray spectrometry in the measurement of naturally occurring radioactive isotopes* (IAEA Training Course Series No. 67). IAEA.

International Atomic Energy Agency. (2020). *Measurement of radioactivity in the environment — Soil — Part 3: Test method of gamma-emitting radionuclides using gamma-ray spectrometry* (ISO 18589-3:2023). IAEA.

International Atomic Energy Agency. (2022). *ALMERA workshop on quality assurance/quality control for environmental radioanalytical laboratories*. IAEA.

International Atomic Energy Agency. (2022). *Intercomparison of k0-NAA software packages* (IAEA-TECDOC-2026). IAEA.

International Atomic Energy Agency. (2023). *ALMERA proficiency tests: Determination of anthropogenic and natural radionuclides in water, soil and simulated contaminated surface samples*. IAEA.

International Atomic Energy Agency. (2024a). *ALMERA training workshops on environmental sampling techniques*. IAEA. https://analytical-reference-materials.iaea.org/almera-workshops

International Atomic Energy Agency. (2024b). *Results of the joint IAEA/EEAE intercomparison exercise on radioanalytical characterization of NORM samples in the European region*. IAEA.

International Atomic Energy Agency. (2024c). *Second interlaboratory comparison on the determination of radionuclides in ALPS treated water*. IAEA.

International Commission on Radiation Units and Measurements. (2006). *Sampling for radionuclides in the environment* (ICRU Report 75). ICRU.

International Commission on Radiological Protection. (2017). *Occupational radiological protection in interventional procedures* (ICRP Publication 139). Elsevier.

International Organization for Standardization. (2007). *Measurement of radioactivity in the environment — Soil — Part 2: Guidance for the selection of the sampling strategy, sampling and pre-treatment of samples* (ISO 18589-2:2007). ISO.

International Organization for Standardization. (2017). *General requirements for the competence of testing and calibration laboratories* (ISO/IEC 17025:2017). ISO.

International Organization for Standardization. (2018). *Soil quality — Sampling — Part 203: Investigation of potentially contaminated sites* (ISO 18400-203:2018). ISO.

International Organization for Standardization. (2023). *Measurement of radioactivity in the environment — Soil — Part 3: Test method of gamma-emitting radionuclides using gamma-ray spectrometry* (ISO 18589-3:2023). ISO.

Knoll, G. F. (2010). *Radiation detection and measurement* (4th ed.). John Wiley & Sons.

Kurnaz, A., Küçükömeroğlu, B., Keser, R., Okumusoglu, N. T., Korkmaz, F., Karahan, G., & Çevik, U. (2007). Determination of radioactivity levels and hazards of soil and sediment samples in Fırtına Valley (Rize, Turkey). *Applied Radiation and Isotopes, 65*(11), 1281–1289. https://doi.org/10.1016/j.apradiso.2007.06.003.

Lakosi, L., Zsigrai, J., Kocsonya, A., Nguyen, T. C., Ramebäck, H., Parsons-Moss, T., Gharibyan, N., & Moody, K. (2018). Gamma spectrometry in the ITWG CMX-4 exercise. *Journal of Radioanalytical and Nuclear Chemistry, 315*(2), 409–416. https://doi.org/10.1007/s10967-017-5667-2

Lawrence Livermore National Laboratory. (2024). Hand-held fast cooling germanium-based radiation detection system. *LLNL-IPO Technology Portal*. https://ipo.llnl.gov/ipo-technologies/national-security-and-defense/hand-held-fast-cooling-germanium-based-radiation

Lin, W. J., & Harbottle, G. (1992). Gamma-ray emission intensities of the thorium-232 chain in secular equilibrium, of uranium-235 and the progeny of uranium-238. *Journal of Radioanalytical and Nuclear Chemistry, 157*, 367–372.

Lucas, S. S. (2021). The Status of NORM and Environmental Exposure in East African Resource Corridors. *International Journal of Current Science Research and Review*, *4*(10), 1260–1275. https://doi.org/10.47191/ijcsrr/v4-i10-10.

Mauz, B., Nolan, P. J., & Appleby, P. G. (2022). Technical note: Quantifying uranium-series disequilibrium in natural samples for dosimetric dating – Part 1: Gamma spectrometry. *Geochronology*, *4*(1), 213–225. https://doi.org/10.5194/gchron-4-213-2022.

Mirion Technologies. (2025). Germanium detectors: Technical specifications and cryogenic cooling systems. *Mirion Technologies Product Documentation*. https://www.mirion.com/products/technologies/spectroscopy-scientific-analysis/gamma-spectroscopy/detectors/hpge-detectors-accessories/germanium-detectors.

Moretti, R., Barresi, A., Chiesa, D., Giachero, A., Labranca, D., Nastasi, M., Paonessa, A., Picione, M., Previtali, E., & Sisti, M. (2024). Machine learning-assisted techniques for Compton-background discrimination in Broad Energy Germanium (BEGe) detector. *arXiv preprint*. https://arxiv.org/abs/2412.08750.

Nguyen, C. T., & Zsigrai, J. (2005). Basic characterization of highly enriched uranium by gamma spectrometry. *Applied Radiation and Isotopes*, *63*(5–6), 687–693. https://doi.org/10.1016/j.apradiso.2005.05.003.

Nguyen, C. T., & Zsigrai, J. (2005). Uncertainty analysis for the determination of the activity concentration of gamma-emitting radionuclides in environmental samples by gamma-ray spectrometry. *Journal of Radioanalytical and Nuclear Chemistry*, *264*(2), 423–431. https://doi.org/10.1007/s10967-005-0736-5.

Nuclear-Power.com. (2022). LN2 cryostat: Cooling of HPGe detectors. *Nuclear Power for Everybody*. https://www.nuclear-power.com/nuclear-engineering/radiation-detection/semiconductor-detectors/high-purity-germanium-detectors-hpge/cooling-of-hpge-detectors/

Ogundare, F. O., & Adekoya, O. I. (2025). Evaluation of natural radioactivity and radiological hazards in soil from Emure-Ekiti, Southwestern Nigeria. *Discover Applied Sciences*, *7*(4), Article 74. https://doi.org/10.1007/s42452-025-06389-4.

Okeji, M. C., Agbalagba, E. O., & Onoja, R. A. (2022). Assessment of radiation hazard indices due to natural radionuclides in soil samples from Imo State University,

Owerri, Nigeria. *Radiation Protection and Environment, 45*(3), 112–120.

Oludoye, O. O., Van den Broucke, S., Chen, X., Supakata, N., Ogunyebi, L. A., & Njoku, K. L. (2023). Identifying the determinants of environmental disposal behavior and policy implications in Nigeria. *Resources, Conservation & Recycling Advances, 18*, 200148. https://doi.org/10.1016/j.rcradv.2023.200148.

ORTEC. (2024). HPGe radiation detector cooling: Cryostats, Dewars, and electro-mechanical options. *ORTEC Technical Documentation*. https://www.ortec-online.com/products/radiation-detectors/high-purity-germanium-hpge-radiation-detectors/detector-cooling

Ravisankar, R., Vanasundari, K., Chandrasekaran, A., Rajalakshmi, A., Suganya, M., Vijayalakshmi, I., & Sivakumar, S. (2012). Measurement of gamma radiation levels in soil samples from Thanjavur using γ-ray spectrometry and estimation of population exposure. *Journal of Medical Physics, 37*(1), 18–22. https://doi.org/10.4103/0971-6203.94951.

Ribeiro, M. F., Costa, C. G. D., & Ramos, F. R. (2024). Exploring Purpose-Driven Leadership: Theoretical Foundations and Impacts in Research Contexts. *Administrative Sciences, 14*, 148. https://doi.org/10.3390/admsci14070148.

Sadeghi, M., Pourimani, R., & Afarideh, H. (2024). Calibration and performance evaluation of an N-type HPGe detector for a collimated and focused PGNAA system by experimental and Monte Carlo methods. *Nuclear Instruments and Methods in Physics Research Section A, 1063*, Article 169310. https://doi.org/10.1016/j.nima.2024.169310

Somashekarappa, H. M., Paramesh, L., Ganesh, A., & Siddappa, K. (2024). Recent advances in gamma-ray spectrometry for environmental monitoring. *Journal of Environmental Radioactivity, 268*, Article 107285. https://doi.org/10.1016/j.jenvrad.2024.107285.

Spahiu, E., Bërdufi, I., & Shyti, M. (2021). Determination of radioactivity in soil samples from Albania. *PoS(BPU11)*, 020. https://pos.sissa.it/427/020/pdf.

Taiwo, A. M., Ogunsola, D. O., Babawale, M. K., Isichei, O. T., Olayinka, S. O., Adeoye, I. A., Adekoya, G. A., & Tayo, O. E. (2023). Assessment of Water Quality Index and the Probable Human Health Implications of Consuming Packaged Groundwater from Southwestern Nigeria. *Sustainability, 15*(4), 3566. https://doi.org/10.3390/su15043566.

Tran, T. N. (2025). Measurement of environmental soil radioactivity using gamma-ray spectrometry. *Salud, Ciencia y Tecnología, 21*(51), Article 2151. https://doi.org/10.56294/saludcyt20252151

Turkat, S., Bemmerer, D., Bootlig, A., Dorulla, A., Koch, J., Lossin, T., Opswald, M., Schmidt, K., & Zuber, K. (2023). Low-background radioactivity counting at the most sensitive HPGe detector in Germany. *TAUP 2023 Conference Proceedings*. https://indico.cern.ch/event/1199289/contributions/5445801/attachments/2705358/4696397/TAUP_2023_Steffen_Turkat.pdf

Tzortzis, M., & Tsertos, H. (2003). Determination of thorium, uranium, and potassium elemental concentrations in surface soils in Cyprus. *Journal of Environmental Radioactivity, 77*(3), 325–338. https://doi.org/10.1016/S0265-931X(03)00074-7.

U.S. Nuclear Regulatory Commission. (2013). *Technical bases and guidance for the use of composite soil sampling for demonstrating compliance with radiological release criteria* (NUREG/CR-7028). NRC.

U.S. Nuclear Regulatory Commission. (2017). *Derivation of the Currie equations* (NUREG/CR-7028). NRC. https://www.nrc.gov/docs/ML1717/ML17178A298.pdf.

Umar, A. M., Ismail, A. F., & Jaafar, M. S. (2021). Efficiency calibration of HPGe detector for gamma-ray spectrometry using Marinelli beaker geometry. *Radiation Physics and Chemistry, 178*, Article 108855. https://doi.org/10.1016/j.radphyschem.2020.108855'

UNSCEAR. (2020). *Sources, effects and risks of ionizing radiation: United Nations Scientific Committee on the Effects of Atomic Radiation 2020 report*. United Nations.

Uwa, J. E. (1984). *Investigation of radiometric anomalies by nuclear and other methods: A case study of the Sokoto Basin, Nigeria* [Unpublished doctoral dissertation]. Ahmadu Bello University.

Wang, Y., Liu, Y., Wu, B., Meng, X., Zhou, L., Ju, A., & Cheng, J. (2025). Design of a multi-layered shield for low-background HPGe spectrometry. *Nuclear Instruments and Methods in Physics Research Section A, 1063*, Article 169310. https://doi.org/10.1016/j.nima.2025.169310.

Wilson, C. A., Matthews, K. L., Hamideh, A. M., & Wang, W. H. (2019). Determination of uranium series activity before secular equilibrium is established. *Health Physics, 117*(4), 449–456. https://doi.org/10.1097/HP.0000000000001073

Yücel, S., Narttürk, R. B., & Gedik, G. (2019). Efficiency calibration of a coaxial HPGe detector–Marinelli beaker geometry using an ^{152}Eu source prepared in epoxy matrix and its validation by efficiency transfer method. *Nuclear Engineering and Technology, 51*(3), 526–533. https://doi.org/10.1016/j.net.2018.09.024.

Zsigrai, J., Nguyen, T. C., & Berlizov, A. (2015). Gamma-spectrometric determination of ^{232}U in uranium-bearing materials. *Applied Radiation and Isotopes, 109*, 509–514. https://doi.org/10.1016/j.apradiso.2015.11.052.